Kobe University Repository : Kernel

PDF issue: 2026-11-21

Effect of chemical composition of coal ash used to prepare granulated coal ash on the removal of hydrogen sulfide from water

Asaoka, Satoshi
Ishidu, Takamichi
Nakamoto, Kenji

(Citation)
Water Environment Research,95(8):e10916

(Issue Date)
2023-08

(Resource Type)
journal article

(Version)
Accepted Manuscript

(Rights)
This is the peer reviewed version of the following article: [Asaoka, S., Ishidu, T., & Nakamoto, K. (2023). Effect of chemical composition of coal ash used to prepare granulated coal ash on the removal of hydrogen sulfide from water. Water Environment Research, 95(8), e10916.], which has been published in final form at…

(URL)
https://hdl.handle.net/20.500.14094/0100485234

Effect of chemical composition of coal ash used to prepare granulated coal ash on the removal of hydrogen sulfide from water

Satoshi ASAOKA [a,b]*, Takamichi ISHIDU [c], Kenji NAKAMOTO [d]

[a] Graduate school of Integrated Sciences for Life, Hiroshima University

1-4-4 Kagamiyama, Higashi-Hiroshima, Hiroshima 739-8528, JAPAN

[b] Research center for Inland Seas, Kobe University

5-1-1 Fukaeminami-machi, Higashinada, Kobe 658-0022, Japan

[c] Graduate School of Maritime Sciences, Kobe University

5-1-1 Fukaeminami-machi, Higashinada, Kobe 658-0022, Japan

[d] The Chugoku Electric Power Co., INC.

4-33, Komachi, Naka-ku, Hiroshima 730-8701, Japan

*Corresponding author:

Tel: +81-82-424-7945, E-mail: stasaoka@hiroshima-u.ac.jp

Abstract

Granulated coal ash was prepared by mixing coal ash derived from a coal electric power plant and blast furnace cement, to remove hydrogen sulfide from aquatic environment. In this study, we investigate the effects of the composition of the coal ash used to prepare the granulated coal ash on its hydrogen sulfide removal performance. Manganese, magnesium, and calcium contents in the granulated coal ash were found to be the major factors in controlling the rate of hydrogen sulfide removal. The kinetics of hydrogen sulfide removal by the granulated coal ash were expressed as a first-order equation with a rate constant of 0.0081– 0.080 h^{-1}. The rate constant for hydrogen sulfide removal obtained in this study correlated well with the manganese content in the granulated coal ash. The increasing surface pH attributed to the hydrolysis of calcium and magnesium on the surface of the granulated coal ash slightly increased the hydrogen sulfide removal rate.

Keywords

Coal ash; Hydrogen sulfide; Manganese oxide; Recycled materials; Wastewater treatment

Introduction

Hydrogen sulfide is generated by sulfate reduction carried out by sulfate-reducing bacteria through anaerobic decomposition of organic matter. In aquatic environment, hydrogen sulfide is commonly detected in wastewater treatment and anoxic sediments in enclosed water bodies (Bonaglia et al., 2019; Stunzhas et al., 2019; Habeeb et al., 2020a; Zwain et al., 2020). In particular, hydrogen sulfide causes toxicity stress for the plants, fishes, and micro-organisms in aquatic ecosystems (Bagarinao, 1992; Lamers et al., 2013; Hancock, 2019) because hydrogen sulfide inhibits the cytochrome c oxidase enzyme in the electron transport chain (Santana Maldonado et al., 2022). Therefore, hydrogen sulfide exerts a negative impact on aquatic organisms even at low concentrations of 0.1-2 mg L^{-1}(Marumo and Yokota, 2012). In addition to the toxicity stress for aquatic ecosystems, the formation of hydrogen sulfide consumes dissolved oxygen in the water column, increasing the sediment oxygen demand (Asaoka et al., 2015; Yamamoto et al., 2016). The depletion of dissolved oxygen in a water column directly affects the respiration of fish and shellfish and, thus, destroys benthic ecosystems. Hence, it is necessary to remove hydrogen sulfide from aquatic environments to maintain healthy aquatic ecosystems.

Composite materials remove environmental pollutants based on their specific

functionality and, thus, have received attention as adsorbents (Ma et al., 2009; Chu et al., 2012; Awual et al., 2019a; Awual et al., 2019b; Pandey et al., 2020; Yu et al., 2021). However, whereas most studies have investigated the removal of hydrogen sulfide gas, only a handful have focused on the removal of liquid-phase hydrogen sulfide. In order to remove hydrogen sulfide from water and sediments, adsorbents prepared from coconut shell, palm kernel shell, wood sawdust (Habeeb et al., 2020b), waste-tire-derived rubber particles (Irfan et al., 2020), δ-MnO_2/porous graphitic carbon (Edathil et al., 2021) and calcined oyster shells (Yamamoto et al., 2022) have been proposed. We previously found that hydrogen sulfide in water can be removed from both fresh water and seawater using granulated coal ash (GCA) prepared from coal fly ash obtained from a coal electric power plant and blast furnace cement (Asaoka et al., 2012; Asaoka et al., 2017). GCA exhibited a high adsorption capacity (>108 mg S g^{-1}) for hydrogen sulfide (Asaoka et al., 2009a) because the GCA sites for hydrogen sulfide adsorption were partially regenerated by oxygen (Asaoka et al., 2014). The adsorption capacity of GCA for hydrogen sulfide exceeded those of functionalized activated carbon (2.7–97.63 mg g^{-1}; Yang et al., 2019; Wang et al., 2020) and amine-modified mesoporous silica (0.034–70 mg g^{-1}; Ma et al., 2009; Chu et al., 2012). This superior adsorption capacity is advantageous for the environmental remediation of organically-enriched coastal sediment with high levels of

hydrogen sulfide. GCA managed to remove hydrogen sulfide simply by scattering it on the organically-enriched coastal sediment (Yamamoto et al., 2016; Jeong et al., 2022). In the semi-field experiment, applying GCA to eutrophic marine sediments significantly decreased the hydrogen sulfide concentration in pore water by 77–100% compared to the control (Asaoka et al., 2009b).

Coal-fired power processes generate more than 500 million tons of fly ash annually (Mathapati et al., 2022). However, only 25% of the total fly ash produced is utilized (Bhatt et al., 2019). As such, current utilization strategies fall short of completely recycling the increasing amount of coal fly ash. Therefore, our proposed novel application that utilizes coal fly ash as an environmental remediation agent for removing hydrogen sulfide is expected to contribute to waste reduction and promote recycling consciousness within society. However, the removal performance of the GCA for hydrogen sulfide may depend on the characteristics of the coal fly ash used to prepare the GCA because coal ash may have a wide range of chemical compositions (e.g., SiO_2 32.04-68.35%; Al_2O_3 11.32-35.23%; Fe_2O_3 0.79-16.44%; CaO 0.43-27.78%; Vassilev et al., 2015). The chemical composition of coal fly ash, obtained from coal fields and the combustion of coal electric power plants, used to prepare the GCA, may vary. Therefore, the objective of this study is to investigate the effects of the characteristics of the coal fly ash used to prepare the

GCA on the removal of hydrogen sulfide from water.

Materials and Methods

Characterization of coal fly ashes to prepare the GCAs

The chemical composition of the coal fly ashes to prepare the GCAs was analyzed by Japanese Industrial Standards (JIS A8815, 2015) and Japan Cement Association standard method (JCAS I-01, 2004).

The pH of the coal fly ashes was measured by the standard method for soil analysis, Japan (Ministry of Agriculture, Forestry and Fisheries, 2023). Briefly, 20 g of the coal fly ash was added to 50 mL of pure water at pH 7 in a 100 mL bottle. The bottle was shaken for 30 min. Thereafter the pH of the liquid phase was measured by a pH electrode.

The Eh–pH diagram of sulfur was illustrated by the geochemical modeling software, Geochemist's Workbench 12.0 (RockWare). The parameters used to illustrate the Eh–pH diagram of sulfur were as follows: the activity of sulfate is set to 0.0031. The pressure and temperature were set at 1013 hPa and 25 °C, respectively.

The loss on ignition (LOI) of the coal fly ashes was measured by Japanese Industrial Standards (JIS A6201, 2015). Briefly, 1 g of coal fly ash was heated at 975℃ until reaching constant weight. LOI was calculated by weighing the coal fly ashes before and

after heating at 975℃.

The Brunauer-Emmett-Teller (BET) specific surface area of the coal fly ashes was measured by nitrogen gas adsorption using a surface area analyzer (ASAP2420; Micromeritics).

Preparation of the GCAs from different coal fly ashes

Three types of coal fly ash provided by the Chugoku Electric Power Co., Inc., Japan, were mixed with blast furnace cement (Class B: Nippon Steel Blast Furnace Slag Cement Co., Ltd, Japan) at a mixture ratio of 85:15 by mass. Water was added to the mixture in the amount of 23-31 wt.%, and subsequently, the mixture was granulated using a rotary pan-type granulator. Every day for the first week, pure water was sprayed onto the surface of the GCA. The GCA was then air-dried under ambient conditions (approximately 25 °C) for 6 months. The prepared GCA was sieved using a sieve with pores of diameter 2–4 mm.

Characterization of the GCAs

The chemical composition of the GCA was analyzed by wavelength dispersive X-ray spectrometry (Supermini 200; Rigaku). The GCA was powdered using an agate mortar.

127 The powdered GCA sample was pressed at 10 MPa to prepare a tablet with a diameter of
128 30 mm. When the tablet was not solidified, Spectro Blend (Chemplex) was added to the
129 powdered GCA as a binder and its total mass was 1 wt.%. The chemical composition of
130 the GCA was determined in the fundamental parameter mode. Total carbon (T-C) and
131 total organic carbon (TOC) in the GCAs were analyzed using an elemental analyzer
132 (JM1000HCN: J-Science Lab).

133 The powder X-ray diffraction pattern of the GCAs was measured using an X-ray
134 diffractometer (XRD-6000; Shimadzu). The GCAs were exposed to the X-ray beam from
135 Cu-Kα radiation at 40 kV and 30 mA. The scanning range of the diffraction angle 2θ was
136 5–80° at a scan rate of 2° min^{-1}. The crystalline materials in the GCAs were identified
137 using a powder diffraction file (JCPDS Card; Joint Committee on Powder Diffraction
138 Standards) and were semi-quantified by the Hanawalt method (Hanawalt et al., 1938).

139 The Brunauer-Emmett-Teller (BET) specific surface area of the GCAs was measured
140 by nitrogen gas adsorption using a surface area analyzer (ASAP2420; Micromeritics).

141 The surface pH of the GCAs was measured using a compact water quality meter
142 (LAQUA twin pH; HORIBA). A CMF filter sheet (Y100A13; Advantec) was placed on
143 the electrode, and the GCAs were placed on the CMF filter. The surface pH of the GCAs
144 was measured by dripping a few drops of ultrapure water onto the GCA.

145

146 ***Removal experiments of hydrogen sulfide using the GCAs***

147 The 10 or 100 mg-S L^{-1} of hydrogen sulfide solution was prepared by dissolving
148 $Na_2S•9H_2O$ (FUJIFILM Wako Chemicals) into de-aerated 30 mmol L^{-1} Tris−HCl buffer.
149 Namely, an aliquot of 1 mol L^{-1} of the Tris−HCl buffer (pH 8; Kanto Kagaku) was diluted
150 by pure water to obtain a concentration of 30 mmol L^{-1}. The Tris−HCl buffer was then
151 de-aerated with purging N_2 gas to a final dissolved oxygen concentration of < 0.2 mg L^{-1}.
152 The prepared hydrogen sulfide solution (50 mL) was gradually dispensed into a 100-
153 mL vial, and the GCA (0.2 g) was added to the solution. Thereafter, the vial was plugged
154 with a rubber cork and sealed with an aluminum cap. The vial was agitated at 100 rpm
155 while kept at 25 °C in a constant-temperature oven. Time evolutions of the hydrogen
156 sulfide concentration were determined using a detection tube (200SA or 200SB: Komyo
157 Rikagaku Kougyo). As a control, the hydrogen sulfide removal experiment without the
158 addition of the GCA was conducted following the same protocol. The batch experiments
159 were conducted in triplicate.

160

161 **Results and Discussion**

162 ***Characteristics of the coal fly ashes to prepare the GCAs***

163 The coal fly ash samples which were used to prepare GCA1 and GCA2 were generated
164 from ultra-supercritical combustion with mixed combustion of Australia and Indonesia
165 coal. By contrast, the GCA3 was prepared from fly ash derived from pulverized coal
166 combustion of Indonesia coal (**Table 1**). The coal fly ashes used in this study were mainly
167 composed of SiO_2 (55.4-60.0 wt.%), Al_2O_3 (20.4-26.5 wt.%), Fe_2O_3 (3.90-6.71 wt.%),
168 CaO (1.01-4.21 wt.%), MgO (0.32-2.38 wt.%), SO_3 (0.32-0.44 wt.%), Na_2O (0.20-0.36
169 wt.%) and K_2O (0.82-1.22 wt.%). The concentration of SiO_2 in the coal fly ashes to
170 prepare the GCAs was higher than that of average from 37 thermo-electric power stations
171 of Spain, Bulgaria, The Netherlands, Italy, Turkey, and Greece (46.6 wt.%; Vassilev and
172 Vassileva, 2007). Because silicic acid react with calcium hydroxide derived from the blast
173 furnace cement through the pozzolanic reaction to prepare the GCA, it is advantageous
174 to prepare the GCA using such a silica rich fly ash.
175 The concentrations of other substances, LOI (2.7-7.6%) and specific surface area (3.01-
176 3.88 $m^2\ g^{-1}$) were within the range of coal fly ash from the 37 thermo-electric power
177 stations (Vassilev and Vassileva, 2007).
178 The pH of fly ash is controlled by the balance of alkaline-earth elements such as CaO
179 and MgO and potentially acid-generating sulfate (Ward et al., 2009). The pH of fly ashes
180 to prepare the GCA2 (pH 4.2) and GCA3 (pH 4.5) was lower than that of GCA1 (pH11.4)

and the average of coal fly ash from the 37 thermo-electric power stations (pH10.0; Vassilev and Vassileva, 2007). This is because calcium concentration of the GCA2 (1.01 wt.%) and GCA3 (1.91 wt.%) is relatively low compared to average of the coal fly ash (7.0 wt.%; Vassilev and Vassileva, 2007). Therefore, the content of alkaline-earth elements in the GCA2 and GCA3 was not sufficient to neutralize sulfate-derived acid.

Characteristics of the GCAs

The GCAs prepared in this study were mainly composed of silicon (21.0-24.5 wt.%), aluminum (10.4-14.0 wt.%), calcium (4.81-7.17 wt.%), iron (2.39-2.87 wt.%) compounds and minor substances (**Table 2**). Environmentally regulated substances such as heavy metals dissolved from the GCA prototype were below the standard levels set by environmental criteria (Asaoka et al., 2008). Therefore, we considered the removal of hydrogen sulfide to be accomplished on the surface of the GCAs and not in the liquid phase. Namely, we previously discovered that the manganese oxide on the surface of the GCA oxidized hydrogen sulfide to sulfur (Asaoka et al., 2012). The manganese concentration in the GCAs was 0.020-0.0439 wt.%.

The LOI values were in the range of 9.22–11.2%. The LOI of the GCA3 (11.2%) was slightly higher compared to that of other samples (9.22%–9.26%; **Table 2**). This is

199 attributed to the higher total organic carbon (TOC) in the GCA3 (5.5%) compared to that
200 in other samples (2.1–4.0%; **Table 2**). In this study, because ignition temperature was
201 975°C, the LOI values represented both organic carbon and carbonate contents (Heiri et
202 al., 2001). However, the inorganic carbon content of the GCAs was less than 1%. Hence,
203 LOI of the GCAs mainly were due to combustion of organic matter originated from coal.
204 The BET specific surface area is one of important parameters for adsorbents. The BET
205 specific surface area of the GCA was 9-10 m^2 g^{-1}, indicating that the value increased by
206 compared to the coal fly ashes (3.01-3.88 m^2 g^{-1}) by mixing the coal ashes with the blast
207 furnace cement (**Table 1 and Table 2**). The BET surface area indicates the reactivity of
208 fly ash by pozzolanic reaction between coal fly ash and cement (Kobayakawa and Habara,
209 2001). The BET specific surface area values of the prepared GCAs are listed in **Table 2**.
210 The BET specific surfacer area of the GCA3 (10 m^2 g^{-1}) was slightly higher compared
211 with others (9 m^2 g^{-1}). A factor in controlling the BET specific surface area of the GCA is
212 the calcium and silicate ratio (C/S ratio). The BET specific surface area of calcium silicate
213 increases with decreasing C/S ratio because of increasing polymerization of the silicate
214 chains (Saito et al., 2017). The C/S ratio of the GCA3 was 0.2, which was lower than
215 others (0.3). Therefore, it is considered that the BET surface area of the GCA3 increased
216 owing to the extension of the silicate chains due to the lower C/S ratio compared with

217 others.

218 The surface pH of GCA1 (pH 9.2) was higher than that of the other GCAs (pH 6.0-
219 6.2). Such a high pH of the GCA1 was attributed to the higher magnesium (1.33 wt.%)
220 and calcium (7.17 wt.%) contents compared to the other GCAs (0.405-0.498 wt.% for
221 magnesium and 4.81–5.31 wt.% for calcium; **Table 2**). It is supported by the fact that the
222 calcium was eluted from the 0-2.50 mm depth from the surface of the GCA (Okuda et al.,
223 2014) and the hydrolysis of calcium hydroxide might increase the surface pH of the GCAs.
224 In contrast, the pH of GCA 2 and GCA3 was pH 6.0-6.2 although those GCAs was
225 prepared from acidic coal fly ashes (pH 4.2-4.5; **Table 1** and **Table 2**), indicating that the
226 calcium hydroxide derived from the blast furnace cement might scavenge proton from the
227 coal fly ashes.

228 The major crystal phases of the GCAs were quartz (36-40%), mullite (28-32%), calcite
229 (18-19%) and corundum (13-14%) (**Table 3** and **Fig. 1**). Additionally, the diffusion ring
230 between 20° and 24° showed the presence of amorphous aluminosilicate and amorphous
231 silica (Li et al., 2009). These crystal phases are frequently found in fly ash (Matsunaga et
232 al., 2002; Chancey et al., 2010). Calcite might be derived from carbonization of calcium
233 hydroxide in the blast furnace cement (Ashraf, 2016). The major crystal phase was similar
234 among the GCAs prepared in this study. Hence, the major crystal phase in the GCAs in

235 this study did not depend on the fly ash originating from different coals.

236

237 ***Removal kinetics of hydrogen sulfide using the GCAs***

238 The hydrogen sulfide concentration decreased faster with the use of GCA1 compared
239 to with the use of GCA2 or GCA3 (**Fig. 2**). For the initial hydrogen sulfide concentration
240 of 100 mg-S L^{-1}, the hydrogen sulfide concentration decreased to 1.0 mg-S L^{-1} after 1 d,
241 whereas the hydrogen sulfide concentrations in GCA2 and GCA3 were still in the 19–25
242 mg-S L^{-1}. The hydrogen sulfide concentration in the control decreased to 6.7 mg-S L^{-1} for
243 the initial concentration of 10 mg-S L^{-1} and to 71 mg-S L^{-1} for the initial concentration of
244 100 mg-S L^{-1}. The decrease of the hydrogen sulfide concentration in the control can be
245 attributed to oxidation and volatilization (Asaoka et al., 2012). The first-order kinetics for
246 hydrogen sulfide shown in **Fig. 3** was corrected by subtracting the decreased in hydrogen
247 sulfide concentration in control from the decrease of hydrogen sulfide concentration in
248 GCAs. The removal kinetics of hydrogen sulfide are well-fit by the first-order equation
249 (Eq. 1; **Fig. 3**). In the case of hydrogen sulfide concentration of 10 mg-S L^{-1}, the first-
250 order rate constant for hydrogen sulfide was calculated within a range of contact time 0–
251 12 h because the most of hydrogen sulfide was removed within 24h.

252

253 $[C_t]=[C_0]e^{-kt}$ ・・・(1)

254

255 The initial rate (R: mg-S L^{-1} h^{-1}) for the removal of hydrogen sulfide is also defined by

256 Eq. 2.

257

258 $R= k [C_0]$ ・・・(2)

259

260 where [Ct] is the hydrogen sulfide concentration at time t (mg-S L^{-1}), $[C_0]$ is the initial

261 concentration of hydrogen sulfide (mg-S L^{-1}), and t is time (h), and k is the first-order rate

262 constant (h^{-1}).

263

264 The rate constants and the initial rate of hydrogen sulfide removal obtained by this

265 study are shown in **Table 4**. The rate constant and the initial rate of hydrogen sulfide

266 removal obtained by the GCA 1 were higher than those of GCA2 and GCA3 under initial

267 concentrations of 10 and 100 mg-S L^{-1}. Those values obtained by the GCA 1 was 2.2–4.2

268 times higher than those of GCA2 and GCA3 for initial concentration of 10 mg-S L^{-1}, and

269 1.5–2.1 times higher than those of GCA2 and GCA3 for initial concentration of 100 mg-

270 S L^{-1}. The major pathway of hydrogen sulfide removal by the GCA is oxidation. Namely,

271 the X-ray absorption fine structure analyses showed that hydrogen sulfide was adsorbed
272 onto the surface of the GCA and successively oxidized to elemental sulfur by the
273 manganese oxide (III) contained in the GCA (Asaoka et al., 2012). The oxidation of
274 hydrogen sulfide was coupled with the reduction of manganese oxide (III) to divalent
275 manganese (Asaoka et al., 2012). The elemental sulfur, derived from the oxidation of
276 hydrogen sulfide, was partially oxidized to sulfate (Asaoka et al., 2012). In contrast,
277 calcium, iron, aluminum, and titanium in the GCA did not play a major role in the removal
278 of hydrogen sulfide (Asaoka et al., 2012). Therefore, the manganese content in GCA is a
279 key parameter for the oxidation of hydrogen sulfide. The rate constant for hydrogen
280 sulfide removal obtained in this study correlated well with the manganese content in the
281 GCAs (r=0.957-0.967; **Fig. 4**). The rate constant for hydrogen sulfide removal increased
282 with increasing manganese content in the GCAs. Hence, we believed that manganese
283 oxide content in the GCA was a major factor in controlling the hydrogen sulfide removal
284 rate. The manganese oxide concentration in fly ashes was 0.03-0.23 wt.% (Vassilev and
285 Vassileva, 2007). Therefore, we can estimate the removal rate of hydrogen sulfide using
286 the manganese content in the GCAs. The manganese in GCAs plays an important role in
287 regenerating the adsorption sites for hydrogen sulfide oxidation. Manganese was reduced
288 through its coupling with hydrogen sulfide oxidation on the surface of the GCAs, then

289 regenerated by dissolved oxygen in the liquid phase. The adsorption site for hydrogen
290 sulfide was regenerated through manganese oxidation at least 10 times under acidic
291 conditions (Asaoka et al., 2014). The rate constant for hydrogen sulfide removal also
292 correlated well with the silicon content in the GCAs (r = 0.993–0.997). However, this
293 correlation is considered spurious correlation because silicon might not oxide hydrogen
294 sulfide directly. One possibility is an increase in the adsorption site for hydrogen sulfide
295 by calcium silicate (Saito et al., 2017).

296 The other possible important parameters for the removal of hydrogen sulfide are the
297 BET-specific surface area, crystal phases, and surface pH. However, both BET specific
298 surface areas and crystal phases of the GCAs did not correlate with the removal rate
299 constant for hydrogen sulfide. Therefore, the BET specific surface area and crystal phases
300 of the GCAs were not considered to be of major importance for the control of the
301 hydrogen sulfide removal rate.

302 The surface pH affects the rate of hydrogen sulfide removal. The Eh–pH diagram of
303 sulfur shows the redox boundary between sulfate and sulfide thermodynamically shifts
304 toward low Eh with increasing pH (**Fig. 5**). Therefore, the hydrogen sulfide on the GCA
305 1 with high surface pH was easy to be oxidized compared to other GCAs. The removal
306 rate of hydrogen sulfide obtained by GCA1, which had a high surface pH, was slightly

307 higher, deviating from the linear regression (**Fig. 4**). As previously mentioned, the surface
308 pH of GCA 1 was 9.2, which was higher than those of the other GCA samples (6.0-6.2)
309 because GCA 1 had higher magnesium and calcium contents compared to the other GCAs
310 (**Table 2**). Although calcium and manganese were considered not to adsorb or oxidize
311 hydrogen sulfide directly, these alkaline-earth elements play an important role in
312 increasing the surface pH of the GCAs. Calcium carbonate, calcium hydroxide derived
313 from calcium oxide, and magnesium hydroxide from magnesium oxide increased OH^-
314 concentration on the surface of GCA1 through the hydrolysis of those alkaline earth
315 substances. Hence, the magnesium and calcium on the surface of GCA1 enhanced the
316 hydrogen sulfide removal rate indirectly.
317
318 **Conclusions**
319 The GCAs prepared from fly ashes originated from different coal and coal electric
320 power generation processes showed a high hydrogen sulfide removal rate in water. Few
321 studies have focused on liquid-phase hydrogen sulfide instead of hydrogen sulfide gas. In
322 this study, we developed a new strategy for utilizing coal fly ash as an environmental
323 remediation material to remove hydrogen sulfide, based on a fly ash and cement
324 composite named GCA. The manganese, magnesium, and calcium contents of the GCAs

were the major factors in controlling the hydrogen sulfide removal rate. Increasing the manganese oxide, which oxidized hydrogen sulfide to elemental sulfur on the surface of the GCAs, enhanced the hydrogen sulfide removal rate. Additionally, raising the surface pH due to the hydrolysis of alkaline earth elements on the surface of the GCAs slightly increased the hydrogen sulfide removal rate. The rate constant for hydrogen sulfide removal obtained in this study correlated well with the manganese content in the GCAs. Hence, the removal rate of hydrogen sulfide by the GCAs can be roughly estimated using the manganese content in the GCAs. Therefore, GCA is a promising strategy for utilizing coal ash.

Acknowledgements

This study was a corroborative research funded by The Chugoku Electric Power Co., Inc. We would like to thank Editage (www.editage.com) for English language editing.

Conflict of interest statement

The funders had no control over the interpretation or publication of this research.

Data availability

343 All data generated or analyzed during this study are included in this published article.

344

345 **References**

346 Asaoka, S., Yamamoto, T., & Yamamoto, K. (2008). A preliminary study of coastal
347 sediment amendment with granulated coal ash – Nutrient elution test and
348 experiment on *Skeletonema costatum* growth – *Journal of Japan Society on Water*
349 *Environment*, 31(8), 455-462. *doi:* 10.2965/jswe.31.455

350 Asaoka, S., Yamamoto, T., & Hayakawa, S. (2009a). Removal of hydrogen sulfide using
351 granulated coal ash. *Journal of Japan Society on Water Environment*, 32(7), 363-
352 368. *doi:* 10.2965/jswe.32.363

353 Asaoka, S., Yamamoto, T., Yoshioka, I., & Tanaka, H. (2009b). Remediation of coastal
354 marine sediments using granulated coal ash. *Journal of Hazardous Materials*,
355 172(1), 92-98. *doi:* 10.1016/j.jhazmat.2009.06.140

356 Asaoka, S., Hayakawa, S., Kim, K. H., Takeda, K., Katayama, M., & Yamamoto, T.
357 (2012). Combined adsorption and oxidation mechanisms of hydrogen sulfide on
358 granulated coal ash. *Journal of Colloid and Interface Science,* 377(1), 284-290. *doi:*
359 10.1016/j.jcis.2012.03.023

360 Asaoka, S., Okamura, H., Akita, Y., Nakano, K., Nakamoto, K., Hino, K., Saito, T.,

361 Hayakawa, S., Katayama, M., & Inada, Y. (2014). Regeneration of manganese
362 oxide as adsorption sites for hydrogen sulfide on granulated coal ash. *Chemical*
363 *Engineering Journal*, 254, 531-537. *doi:* 10.1016/j.cej.2014.06.005
364 Asaoka, S., Yamamoto, T., Yamamoto, H., Okamura, H., Hino, K., Nakamoto, K., &
365 Saito, T. (2015). Estimation of hydrogen sulfide removal efficiency with granulated
366 coal ash applied to eutrophic marine sediment using a simplified simulation model.
367 *Marine Pollution Bulletin,* 94(1-2), 55-61. *doi:* 10.1016/j.marpolbul.2015.03.017
368 Asaoka, S., Okamura, H., Kim, K., Hatanaka, Y., Nakamoto, K., Hino, K., Oikawa, T.,
369 Hayakawa, S., & Okuda, T. (2017). Optimum reaction ratio of coal fly ash to blast
370 furnace cement for effective removal of hydrogen sulfide. *Chemosphere*, 168, 384-
371 389. *doi:* 10.1016/j.chemosphere.2016.10.070
372 Ashraf, W. (2016). Carbonation of cement-based materials: Challenges and
373 opportunities. *Construction and Building Materials*, 120, 558-570. *doi:*
374 10.1016/j.conbuildmat.2016.05.080
375 Awual, M. R. (2019a). Novel ligand functionalized composite material for efficient
376 copper (II) capturing from wastewater sample. *Composites Part B: Engineering*,
377 172, 387-396. *doi:* 10.1016/j.compositesb.2019.05.103
378 Awual, M. R., Hasan, M. M., Asiri, A. M., & Rahman, M. M. (2019b). Cleaning the

379 arsenic (V) contaminated water for safe-guarding the public health using novel
380 composite material. *Composites Part B: Engineering*, 171, 294-301. *doi*:
381 10.1016/j.compositesb.2019.05.078
382 Bagarinao, T. (1992). Sulfide as an environmental factor and toxicant. tolerance and
383 adaptations in aquatic organisms. *Aquatic Toxicology*, 24(1-2), 21-62. doi:
384 10.1016/0166-445X(92)90015-F
385 Bhatt, A., Priyadarshini, S., Mohanakrishnan, A. A., Abri, A., Sattler, M., &
386 Techapaphawit, S. (2019). Physical, chemical, and geotechnical properties of coal
387 fly ash: A global review. *Case Studies in Construction Materials*, 11, e00263. *doi:*
388 10.1016/j.cscm.2019.e00263
389 Bonaglia, S., Marzocchi, U., Ekeroth, N., Brüchert, V., Blomqvist, S., & Hall, P. O.
390 (2019). Sulfide oxidation in deep Baltic Sea sediments upon oxygenation and
391 colonization by macrofauna. *Marine Biology*, 166, 1-12. *doi:* 10.1007/s00227-019-
392 3597-y
393 Chancey, R. T., Stutzman, P., Juenger, M. C., & Fowler, D. W. (2010). Comprehensive
394 phase characterization of crystalline and amorphous phases of a Class F fly ash.
395 *Cement and Concrete Research*, 40(1), 146-156. *doi:*
396 10.1016/j.cemconres.2009.08.029

397 Chu, X., Cheng, Z., Zhao, Y., Xu, J., Zhong, H., Zhang, W., Lü, J., Zhou, S., Zhu, F.,
398 Zhou, Y. & Zhou, L. (2012). Study on sorption behaviors of H_2S by
399 triethanolamine-modified mesoporous molecular sieve SBA-15. *Industrial &*
400 *Engineering Chemistry Research*, 51(11), 4407-4413. *doi:* 10.1021/ie202360h
401 Edathil, A. A., Kannan, P., Haija, M. A., & Banat, F. (2021). Sulfide remediation from
402 wastewater using hydrothermally synthesized δ-MnO_2/porous graphitic carbon as
403 adsorbent. *Environmental Research*, 196, 110429. *doi:*
404 10.1016/j.envres.2020.110429
405 Habeeb, O. A., Olalere, O. A., Kanthasamy, R., & Ayodele, B. V. (2020a). Hydrogen
406 sulfide removal from downstream wastewater using calcium-coated wood
407 sawdust-based activated carbon. *Arabian Journal for Science Engineering*, 45(2),
408 501-518. *doi:* 10.1007/s13369-019-04207-9
409 Habeeb, O. A., Kanthasamy, R., Saber, S. E. M., & Olalere, O. A. (2020b).
410 Characterization of agriculture wastes based activated carbon for removal of
411 hydrogen sulfide from petroleum refinery waste water. *Materials Today:*
412 *Proceedings*, 20, 588-594. *doi:* 10.1016/j.matpr.2019.09.194
413 Hanawalt, J. D., Rinn, H. W., & Frevel, L. K. (1938). Chemical analysis by X-ray
414 diffraction. *Industrial & Engineering Chemistry Analytical Edition*, 10(9), 457-

512.

Hancock, J. T. (2019). Hydrogen sulfide and environmental stresses. *Environmental and Experimental Botany*, 161, 50-56. *doi:* 10.1016/j.envexpbot.2018.08.034

Heiri, O., Lotter, A.F. & Lemcke, G. (2001) Loss on ignition as a method for estimating organic and carbonate content in sediments: reproducibility and comparability of results. *Journal of Paleolimnology* 25, 101–110. *doi:* 10.1023/A:1008119611481

Irfan, M., Siddiqui, M., Bashir, F., Butt, M. T., & Abbas, N. (2020). Efficient removal of hydrogen sulfide from wastewater using waste-tire-derived rubber particles. *International Journal of Environmental Science and Technology*, 17, 3515-3524. *doi:* 10.1007/s13762-020-02724-x

Japanese Industrial Standards (2015) JIS A6201. Retrieved from https://www.jisc.go.jp/app/jis/general/GnrJISSearch.html (in Japanese)

Japanese Industrial Standards (2015) JIS A8815. Retrieved from https://www.jisc.go.jp/app/jis/general/GnrJISSearch.html (in Japanese)

Japan Cement Association (2004) JCAS method. Retrieved from https://www.jcassoc.or.jp/cement/1jpn/jj3g.html#13 (in Japanese)

Jeong, I., Nakashita, S., Hibino, T., & Kim, K. (2022). Effect of sediment deposition on phosphate and hydrogen sulfide removal by granulated coal ash in coastal

433 sediments. *Marine Pollution Bulletin*, 179, 113679.
434 *doi:*10.1016/j.marpolbul.2022.113679
435 Kobayakawa, M., Habara, S. (2001) Changes in porosity and microstructure of hardened
436 body derived from pozzolanic reaction of fly ash. *Proceedings of the Japan*
437 *Concrete Institute* 23(2), 97-102. (in Japanese)
438 Lamers, L. P., Govers, L. L., Janssen, I. C., Geurts, J. J., Van der Welle, M. E., Van
439 Katwijk, M. M., Heide, T. V., Roelofs, J. G. M., & Smolders, A. J. (2013). Sulfide
440 as a soil phytotoxin—a review. *Frontiers in Plant Science,* 4, 268. *doi:*
441 10.3389/fpls.2013.00268
442 Li, J., Lin, H., Li, J., & Wu, J. (2009) Effects of different potassium salts on the formation
443 of mullite as the only crystal phase in kaolinite. *Journal of European Ceramic*
444 *Society*, 29(14), 2929-2936. *doi:* 10.1016/j.jeurceramsoc.2009.04.032
445 Ma, X., Wang, X., & Song, C. (2009). "Molecular basket" sorbents for separation of
446 CO_2 and H_2S from various gas streams. *Journal of the American Chemical Society*,
447 131(16), 5777-5783. *doi:* 10.1021/ja8074105
448 Marumo, K. & Yokota, M. (2012). Review on aoshio and biological effects of hydrogen
449 sulfide, *Report of Marine Ecology Research Institute,* 15, 23–40. (in Japanese)
450 Mathapati, M., Amate, K., Prasad, C. D., Jayavardhana, M. L., & Raju, T. H. (2022). A

451 review on fly ash utilization. *Materials Today: Proceedings*, 50, 1535-1540. doi:
452 10.1016/j.matpr.2021.09.106
453 Matsunaga, T., Kim, J. K., Hardcastle, S., & Rohatgi, P. K. (2002). Crystallinity and
454 selected properties of fly ash particles. *Materials Science and Engineering: A*,
455 325(1-2), 333-343. doi: 10.1016/S0921-5093(01)01466-6
456 Ministry of Agriculture, Forestry and Fisheries (2023, March 23) The standard method
457 for soil analysis. Retrieved from
458 https://www.maff.go.jp/j/seisan/kankyo/hozen_type/h_sehi_kizyun/attach/pdf/i
459 baraki01-4.pdf (in Japanese)
460 Okuda, T., Asaoka, S., Yano, H., Yoshitsugu, K., Nakai, S., Nishijima, W., Sugimoto, K.,
461 Matsunami, D., Asaoka, Y., & Okada, M. (2014). Chemical behavior of sand
462 alternatives in the marine environment. *Chemosphere*, 111, 164-168. *doi:*
463 10.1016/j.chemosphere.2014.03.075
464 Pandey, S., Fosso-Kankeu, E., Spiro, M. J., Waanders, F., Kumar, N., Ray, S. S., Kim, J.
465 & Kang, M. (2020). Equilibrium, kinetic, and thermodynamic studies of lead ion
466 adsorption from mine wastewater onto MoS_2-clinoptilolite composite. *Materials*
467 *Today Chemistry*, 18, 100376. *doi:* 10.1016/j.mtchem.2020.100376
468 Saito, T., Sato, K., Tsuruki, T., Saeki, T. (2017). Effect of C/S ratio and aluminum

substitution on hydrogen sulfide adsorption mechanism of calcium silicate hydrates. *Cement Science and Concrete Technology*, 71, 101-108. *doi:* 10.14250/cement.71.101(in Japanese with English abstract)

Santana Maldonado, C., Weir, A., & Rumbeiha, W. K. (2022). A comprehensive review of treatments for hydrogen sulfide poisoning: past, present, and future. T*oxicology Mechanisms and Methods*, 33(3), 183-196. *doi:* 10.1080/15376516.2022.2121192

Stunzhas, P. A., Gulin, M. B., Zatsepin, A. G., & Ivanova, E. A. (2019). On the possible presence of oxygen in the upper sediment layer of the hydrogen sulfide zone in the Black Sea. *Oceanology*, 59(1), 155-157. *doi:* 10.1134/S0001437019010211

Vassilev, S. V., & Vassileva, C. G. (2007). A new approach for the classification of coal fly ashes based on their origin, composition, properties, and behaviour. *Fuel*, 86(10-11), 1490-1512. *doi:* 10.1016/j.fuel.2006.11.020

Vassilev, S. V., Vassileva, C. G., & Vassilev, V. S. (2015). Advantages and disadvantages of composition and properties of biomass in comparison with coal. An overview. *Fuel*, 158, 330-350. *doi:* 10.1016/j.marpolbul.2022.113679

Wang, S., Nam, H., & Nam, H. (2020). Preparation of activated carbon from peanut shell with KOH activation and its application for H_2S adsorption in confined space.

Journal of Environmental Chemical Engineering, 8(2), 103683. *doi:* 10.1016/j.jece.2020.103683

Ward, C. R., French, D., Jankowski, J., Dubikova, M., Li, Z., & Riley, K. W. (2009). Element mobility from fresh and long-stored acidic fly ashes associated with an Australian power station. *International Journal of Coal Geology*, 80(3-4), 224-236. *doi:* 10.1016/j.coal.2009.09.001

Yamamoto, H., Yamamoto, T., Mito, Y., & Asaoka, S. (2016). Numerical evaluation of the use of granulated coal ash to reduce an oxygen-deficient water mass. *Marine Pollution Bulletin,* 107(1), 188-205. *doi:* 10.1016/j.marpolbul.2015.03.017

Yamamoto, T., Nakajima, T., & Asaoka, S. (2022). Changes in physical and chemical characteristics and reactivity to hydrogen sulfide of calcined oyster shells. *Fisheries Science*, 88(5), 609-616. *doi:* 10.1007/s12562-022-01620-2

Yang, C., Yang, S., Fan, H., Wang, Y., & Shangguan, J. (2019). Tuning the ZnO-activated carbon interaction through nitrogen modification for enhancing the H_2S removal capacity. *Journal of Colloid and Interface Science*, 555, 548-557. *doi:* 10.1016/j.jcis.2019.08.014

Yu, F., Bai, X., Liang, M., & Ma, J. (2021). Recent progress on metal-organic framework-derived porous carbon and its composite for pollutant adsorption from

liquid phase. *Chemical Engineering Journal*, 405, 126960. *doi:* 10.1016/j.cej.2020.126960

Zwain, H. M., Nile, B. K., Faris, A. M., Vakili, M., & Dahlan, I. (2020). Modelling of hydrogen sulfide fate and emissions in extended aeration sewage treatment plant using TOXCHEM simulations. *Scientific Reports*, 10(1), 1-11. *doi:* 10.1038/s41598-020-79395-8

Figures

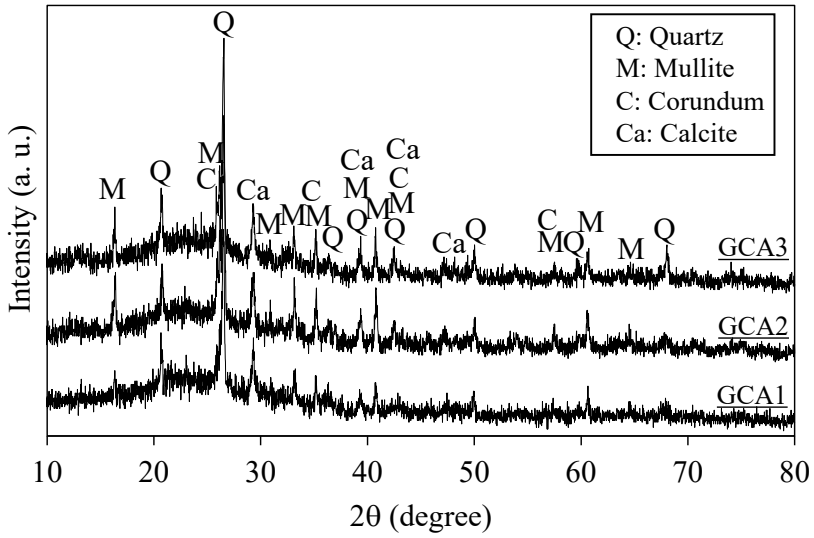


Fig. 1 Powder X-ray diffraction patterns of the GCAs

The major crystal phases of the GCAs were quartz, mullite, corundum and calcite.

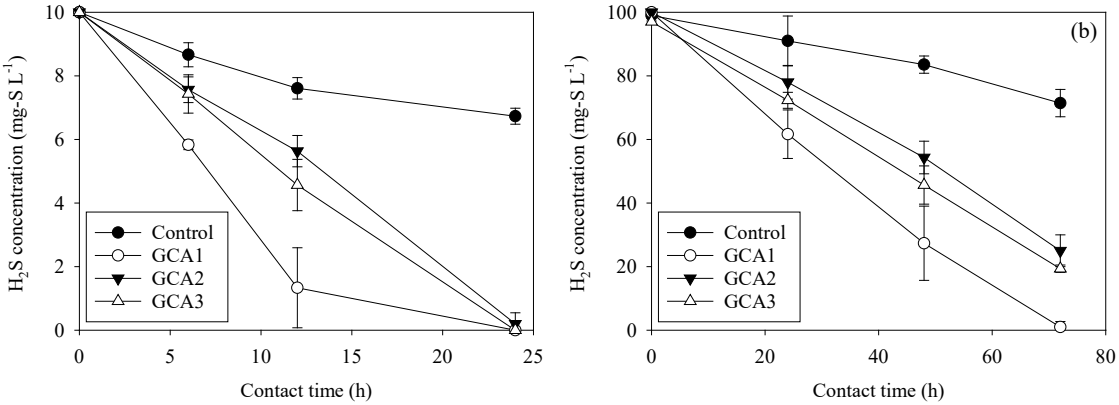


Fig. 2 Time evolutions of hydrogen sulfide concentration after addition of the GCAs.

Initial concentration of hydrogen sulfide was 10 mg-S L^{-1} (a) and 100 mg-S L^{-1} (b). Error bars indicate standard deviations. The hydrogen sulfide concentration decreased faster with the use of GCA 1 compared to with the use of GCA 2 or GCA 3

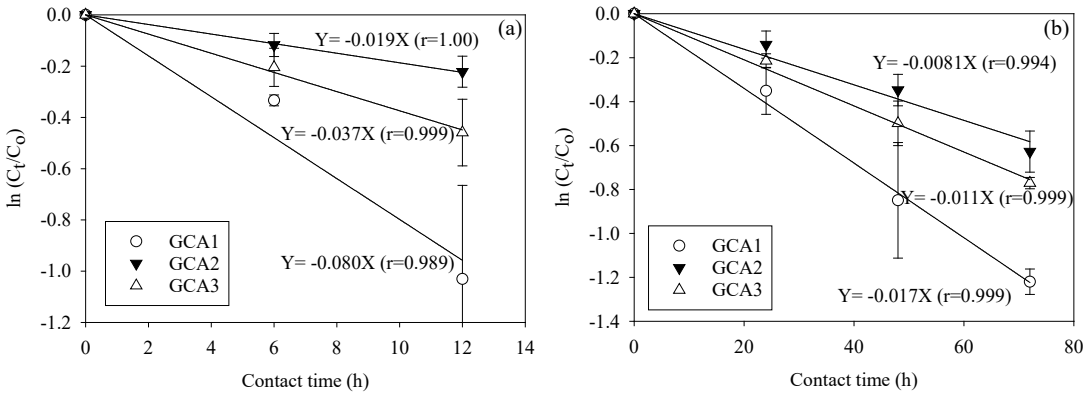


Fig. 3 The first-order removal kinetics of hydrogen sulfide using the GCAs.

Initial concentration of hydrogen sulfide was 10 mg-S L^{-1} (a) and 100 mg-S L^{-1} (b). Error bars indicate standard deviations. The removal kinetics of hydrogen sulfide are well-fit by the first-order equation.

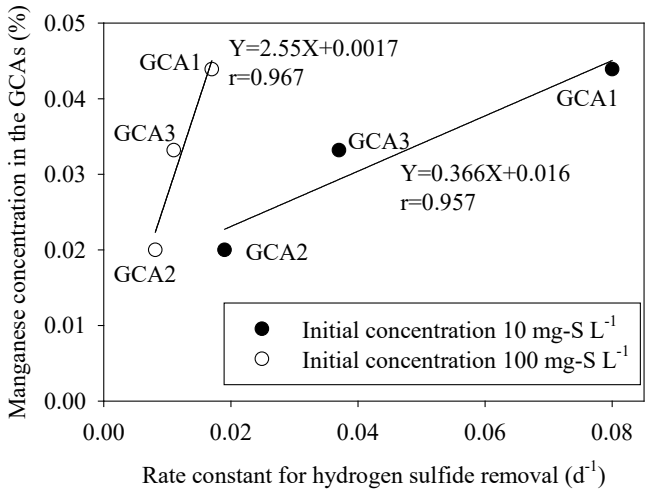


Fig. 4 The relationship between the rate constant for hydrogen sulfide removal and manganese content in the GCAs.

The rate constant for hydrogen sulfide removal correlated well with the manganese content in the GCAs.

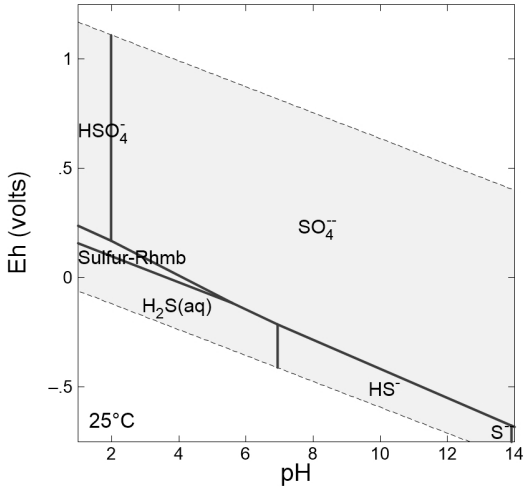


Fig. 5. Eh–pH diagram of sulfur

The redox boundary between sulfate and sulfide thermodynamically shifts toward low Eh with increasing pH.

Table 1 Characteristics of fly ashes to prepare the GCAs tested in this study

	GCA1	GCA2	GCA3
System on coal electric power plant	Ultra Super Critical	Ultra Super Critical	Pulverized coal firing
Origin of coal and mixed combustion ratio (%)	Australia (70%) Indonesia (30%)	Australia (40%) Indonesia (60%)	Indonesia (100%)
SiO_2 (%)	60.0	55.4	56.0
Al_2O_3 (%)	20.4	26.5	21.6
Fe_2O_3 (%)	4.02	3.90	6.71
CaO	4.21	1.01	1.91
MgO	2.38	0.32	1.65
SO_3	0.44	0.32	0.34
Na_2O	0.20	0.27	0.36
K_2O	0.82	1.03	1.22
Loss on ignition (%)	2.7	5.0	7.6
pH	11.4	4.2	4.5
BET specific surface area ($m^2\ g^{-1}$)	3.48	3.01	3.88

Table 2 Chemical composition of GCAs tested in this study

Concentration (wt%)	GCA1	GCA2	GCA3
Inorganic carbon	0.7	1.0	0.9
Total organic carbon	2.1	4.0	5.5
Mg	1.33	0.405	0.498
Al	10.4	14.0	11.1
Si	24.5	21.0	22.4
P	0.136	0.137	0.0991
S	0.447	0.329	0.309
Cl	0.0131	0.0073	0.0052
K	0.672	0.818	1.03
Ca	7.17	5.31	4.81
Ti	0.541	0.789	0.541
Mn	0.0439	0.020	0.0332
Fe	2.87	2.39	2.84
Ni	0.0434	0.0119	0.0123
Cu	0.0144	0.0125	0.0118
Zn	0.0164	0.0188	0.0165
Ge	0.0084	<0.004	<0.004
Rb	<0.003	<0.003	0.0081
Sr	0.159	0.0935	0.0541
Y	0.0116	0.0052	<0.003
Zr	0.143	0.0426	0.0371
Ba	0.196	<0.05	<0.05
Others	4.77	8.5	9.7
Loss on ignition (%)	9.26	9.22	11.2
Surface pH	9.2	6.2	6.0
BET specific surface area ($m^2 g^{-1}$)	9	9	10

Table 3 Percent composition of major crystal phases of GCAs tested in this study (%)

Crystal Phases	GCA1	GCA2	GCA3
SiO_2	37	36	40
$Al_6Si_2O_{13}$	30	32	28
$CaCO_3$	19	18	19
Al_2O_3	14	14	13

Table 4 Rate constant and initial rate for hydrogen sulfide removal

	Initial H_2S: (10 mg-S L^{-1})		Initial H_2S: (100 mg-S L^{-1})	
	k (h^{-1})	(R: mg-S L^{-1} h^{-1})	k (h^{-1})	(R: mg-S L^{-1} h^{-1})
GCA 1	0.080*	0.80*	0.017**	1.7**
GCA 2	0.019	0.19	0.0081	0.81
GCA 3	0.037	0.37	0.011	1.1

**: $p<0.01$; *: $p<0.05$